Available online at www.sciencedirect.com
ScienceDirect
Lithos 99 (2007) 25–44
LITHOS
www.elsevier.com/locate/lithos

The metasomatic record in the shallow peridotite mantle beneath Grenada (Lesser Antilles arc)

R. Vannucci [a,b,*], M. Tiepolo [b], M.J. Defant [c], P. Kepezhinskas [d]

[a] *Dipartimento di Scienze della Terra, Università di Pavia, Pavia, Italy*
[b] *Istituto di Geoscienze e Georisorse, CNR, Sezione di Pavia, Pavia, Italy*
[c] *Department of Geology, University of South Florida, Tampa, FL 33620, USA*
[d] *9303 Brookhurst Court, Tampa, FL 33647, USA*

Received 23 May 2006; accepted 15 May 2007
Available online 8 June 2007

Abstract

The composition and geochemical signatures of the mantle wedge beneath the Lesser Antilles arc are documented by the ultramafic xenoliths included in alkali basalts (M-series) on Grenada. Xenoliths consist of harzburgites, lherzolites, dunites and subordinate wehrlites and pyroxenites. Primary minerals phases are olivine, low-Al and high-Al orthopyroxene, clinopyroxene and Cr-Spinel. In addition to the primary assemblage, Grenada xenoliths contain metasomatic phases such as Al-rich clinopyroxene, plagioclase, Al-rich spinel, pargasitic amphibole and Si- and Al-rich glasses. The trace-element signatures of pyroxenes and glasses have been determined on selected samples by LA-ICP-MS. Pyroxenes from both lherzolite and harzburgite xenoliths have U-shaped rare earth element (REE) profiles, unusually high Th, U and Sr concentrations and large negative Nb, Ta and Zr, and Hf anomalies. The geochemical signatures of metasomatic clinopyroxene are different from those reported for clinopyroxene from fluid-metasomatised mantle wedge, and are clearly distinct from those of clinopyroxene in equilibrium with host lavas. Si-rich glasses show a narrow compositional range, with trace-element characteristics closely similar to those of reacted pyroxenes. This, along with the general lack of chemical gradients of LILE and LREE over more compatible elements suggests dacitic glasses represent the products of in-situ melting caused by temperature increase before and during the uptake of xenoliths by host lavas. Dacitic melts are believed to represent local re-melts of regions metasomatically enriched by earlier arc magmas that had stalled, fractionated, and solidified in the upper mantle. These local re-melts thus reflect the metasomatic component formed by earlier arc-related metasomatic agents and liable to be re-mobilised. This also appears to be the easiest way to explain the compositional similarities between erupted arc lavas and the metasomatised peridotites.

The results of this study suggest that the mantle wedge beneath the Lesser Antilles underwent complex peridotite–melt reaction processes operated by sub-arc melts and, later on, by magmas similar in compositions to the host alkali basalts. The majority of the compositional range of erupted Grenada magmas, but adakites found at surface, can be obtained by the interaction of basalts, possibly formed by hydrous melting of MORB-source mantle, with the overlying mantle wedge.
© 2007 Elsevier B.V. All rights reserved.

Keywords: Sub-arc mantle; Mantle xenoliths; Metasomatism; Clinopyroxene; Glasses; Lesser Antilles; LA-ICP-MS

* Corresponding author. Dipartimento di Scienze della Terra, Università di Pavia, via Ferrata 1, I-27100 Pavia, Italy. Tel.: +39 0382 985884; fax: +39 0382 985890.
E-mail address: vannucci@crystal.unipv.it (R. Vannucci).

0024-4937/$ - see front matter © 2007 Elsevier B.V. All rights reserved.
doi:10.1016/j.lithos.2007.05.007

Table 1
Representative major element (wt.%) compositions of olivine

Rock type	Wh	Du	Du	Du	Hz	Hz	Hz	Hz	Hz	Hz	Hz	Lh	Lh	Lh	Wb	Wb	Wb	Py
Sample	gr 7–1	gr 7–2	gr 1	gr 20b	gr 20–22	gr 20–15a	gr 20–8a	gr 1–2	gr 5–1	gr 20–9c	gr 20–15	gr 20–90	gr 20–21	gr 20–15b	gr 20–2	gr 20–10	gr 20–13	gr 20–13	gr 20–8c
SiO_2	39.49	40.94	40.90	40.30	41.62	40.86	40.54	40.43	41.38	41.91	40.68	40.15	40.72	41.30	41.01	41.17	41.70	40.78	41.67
TiO_2	–	0.02	0.05	–	–	–	–	–	–	–	–	–	–	–	–	–	–	–	–
Cr_2O_3	–	0.06	–	–	–	0.06	–	–	–	–	–	–	–	–	–	–	–	–	–
FeO_{tot}	16.64	10.13	12.70	10.14	9.92	11.09	10.36	13.56	8.63	9.84	10.12	12.22	9.94	10.32	12.71	10.74	11.00	12.29	9.52
MnO	0.15	0.03	0.11	–	–	–	0.04	0.06	0.01	0.03		0.08	–	–	0.02	–	–	0.05	–
NiO	0.37	0.10	0.19	0.40	0.23	0.29	0.39	0.15	0.39	0.32	0.75	0.24	0.64	0.78	0.11	0.29	0.24	0.13	0.35
MgO	43.57	47.74	46.55	49.14	47.21	47.63	47.72	45.99	50.20	48.54	48.64	47.03	48.71	47.47	45.64	48.11	46.94	46.89	47.80
CaO	0.26	0.06	0.04	0.03	0.01	0.03	–	0.01	0.03	0.05	0.11	0.03	–	–	0.16	0.16	0.03	0.15	0.04
Na_2O	–	–	0.08	–	–	–	–	0.15	–	–	–	–	–	–	–	–	0.04	0.01	0.01
Sum	100.5	99.08	100.6	100.0	98.99	99.96	99.05	100.4	100.6	100.7	100.3	99.75	100.0	99.87	99.65	100.5	99.95	100.3	99.39
Fo	0.82	0.88	0.86	0.90	0.87	0.87	0.88	0.85	0.91	0.88	0.89	0.87	0.89	0.87	0.85	0.88	0.86	0.86	0.875

– Below detection limits; Wh = wehrlite; Du = dunite; Hz = harzburgite; Lh = lherzolite; Wb = websterite; Py = pyroxenite.

1. Introduction

Mantle xenoliths are relatively rare in the magmatic products of volcanic arcs, thus preventing direct chemical information on the composition of the mantle wedge and on the role of slab-derived fluids and/or melts in the modification of the mantle's original geochemical signatures. Sub-arc xenoliths from intra-oceanic island arcs, excluding fore-arc and back-arc xenoliths, have been described from Lihir and Simberi Islands, Papua New Guinea (McInnes and Cameron, 1994; Eiler et al., 1998; McInnes et al., 1999, 2001; Grégoire et al., 2001), Batan Island, Philippines (Vidal et al., 1989; Maury et al., 1992; McInnes and Cameron, 1994; Eiler et al., 1998; McInnes et al., 1999, 2001; Grégoire et al., 2001), Kurile, Russia (Swanson et al., 1987; Kepezhinskas et al., 1995, 1996; Kepezhinskas and Defant, 1996, 2001; Kepezhinskas et al., 2002), Grenada, Lesser Antilles (Arculus and Wills, 1980; Defant et al., 2000; Parkinson et al., 2003), Marelava Volcano, Vanuatu Arc (Barsdell and Smith, 1989; Parkinson and Arculus, 1999) and the Aleutian Arc (DeLong et al., 1975; Conrad and Kay, 1984; Debari et al., 1987; Swanson et al., 1987).

On Grenada two major groups of mafic lavas occur: i) the C-series basalts (calcic and clinopyroxene-phyric, broadly corresponding to ankaramites; Thirlwall and Graham, 1984; Thirlwall et al., 1996), which give rise by differentiation to calc-alkaline andesites and dacites; and ii) M-series basalts (magnesian and olivine-microphyric) from which a series of low-Ca, low-Fe, high-SiO_2 basalts and mafic andesites derives.

Microphyric alkali olivine basalts from the M-series occasionally contain Na-metasomatised mantle xenoliths and present us with the opportunity to acquire petrologic and geochemical data for the sub-arc mantle. We believe the xenoliths are a key to understanding the nature and composition of subduction-related metasomatic agents, and the chemical effects of their interaction with sectors of the mantle wedge. Moreover, these xenoliths may also offer precious insights into the possible links between lithospheric mantle, erupted adakites, and alkali basalts in the arc environment.

A summary of the petrology, mineralogy and geochemistry of the Grenada xenolith suite has been presented recently by Parkinson et al. (2003), along with a discussion of the implications of the data with respect to sub-arc mantle processes. We present in this paper new results of detailed in-situ laser ablation-inductively coupled plasma-mass spectrometry (LA-ICP-MS) investigations of pyroxenes and glasses from Grenada xenoliths. The data presented here provide additional

Table 2
Representative major element (wt.%) compositions of orthopyroxene

Rock type	Du	Hz	Hz	Hz	Hz	Hz	Hz	Hz	Hz	Lh	Lh	Lh	Wb	Wb	Lh	Py
Sample	gr 1	gr 20–22	gr 20–15a	gr 1–5	gr 1–2	gr 20–8a	gr 5–1	gr 20–9c	gr 20–90	gr 20–21	gr 20–15b	gr 20–2	gr 20–10	gr 20–13	gr 20–9a	gr 20–8c
SiO_2	56.62	48.58	56.85	57.56	57.21	57.84	57.92	57.79	55.53	56.98	56.43	58.5	58.99	57.33	58.46	55.36
TiO_2	0.07	–	–	–	–	0.08	–	0.02	0.05	0.03	–	–	–	–	–	0.04
Al_2O_3	2.28	9.73	2.08	1.27	1.45	0.62	2.09	0.52	3.05	3.07	3.31	0.32	0.07	1.26	0.26	4.03
Cr_2O_3	0.23	1.86	–	0.54	0.01	0.03	–	0.09	0.18	0.63	0.45	–	–	0.01	–	0.35
FeO_{tot}	8.51	7.42	6.89	5.5	8.83	6.84	6.36	6.77	8.89	6.72	6.92	6.51	6.37	7.41	6.91	6.41
MnO	0.13	–	–	–	0.15	0.06	–	0.10	0.07	–	–	–	–	0.05	–	–
NiO	0.03	0.07	0.01	0.04	–	0.02	0.13	0.01	–	–	0.14	0.07	0.06	0.04	0.18	0.03
MgO	30.80	28.80	32.94	32.7	31.65	34.4	33.02	34.11	31.41	31.45	31.65	34.25	34.35	33.04	33.54	30.82
CaO	0.91	3.55	0.54	1.68	0.5	0.18	0.45	0.17	0.30	0.60	0.58	0.16	0.09	0.22	0.18	3.28
Na_2O	–	0.03	0.01	0.06	0.03	–	–	0.02	–	–	–	0.02	–	0.07	0.02	–
K_2O	0.02	0.02	0.02	0.05	0.05	0.01	–	0.02	0.02	0.02	0.01	0.01	0.02	0.02	0.01	0.04
Sum	99.6	100.1	99.34	99.4	99.88	100.1	99.97	99.62	99.5	99.5	99.49	99.84	99.95	99.45	99.56	100.4
Mg#	0.87	0.87	0.89	0.91	0.86	0.90	0.90	0.90	0.86	0.89	0.89	0.90	0.91	0.89	0.90	0.90

– Below detection limits; Wh = wehrlite; Du = dunite; Hz = harzburgite; Lh = lherzolite; Wb = websterite; Py = pyroxenite.

chemical information aimed at better constraining the metasomatic history of the sub-arc mantle beneath the southern terminus of the Lesser Antilles arc, and at recognising in mantle pyroxenes geochemical signatures that can be unquestionably related to slab-derived metasomatic agents.

2. Geologic background

Grenada is located at the southern terminus of the Lesser Antilles arc where magmatism is caused by subduction of Atlantic oceanic lithosphere beneath the leading edge of the Caribbean plate. The latter probably formed in the Pacific during the Cretaceous and was emplaced between the North and South American plates by Late Eocene time (Waggoner, 1987; Pindell and Barret, 1990). The subducting slab beneath Grenada terminates abruptly along the continental platform of South America. The close proximity of Grenada to the giant transform fault bounding the southern Caribbean plate may imply that the velocity of the convecting wedge flow approach zero and, in turn, that the slower convecting wedge has larger time-integrated contributions of fluid and is hotter than faster convecting regions. On the other hand, the edge of the torn slab beneath Grenada might be elevated in temperature due to the contact with the hot mantle below the continental platform (Defant et al., 2000), thus possibly inducing melting of the slab.

In Grenada, five major volcanic centres have been identified (Arculus, 1976), although the relative ages are still poorly known. Miocene ages are inferred for the Mt. Morice–Mt. Maitland and the Southeast Mountain volcanic centres, whereas Pliocene–Pleistocene ages have been recognised at Mt. Granby–Fedon's Camp and Mt. St. Catherine (Briden et al., 1979). Older ages are not confirmed by recently obtained age determinations which are mostly <1 Ma, and certainly no older than 3 Ma (Thirlwall and Graham, 1984; Speed et al., 1993).

3. Petrography

The composition and geochemical signatures of the mantle wedge beneath Grenada are documented by the abundant ultramafic xenoliths included in M-series basalts from Queens Park and Grenville (Parkinson et al., 2003). Both xenolith sites are dominated by harzburgite (50%), followed by dunite (15%) and lherzolite (15%), with subordinate wehrlites, websterite and pyroxenite (up to 20%). No garnet-bearing assemblages have been detected. As for texture and mode, the investigated samples closely match those described by Parkinson et al. (2003).

Spinel-bearing harzburgite (samples gr 20–22, gr 20–15a, gr 20–8a, gr 1–2, gr 1–5, gr 5–1, gr 20–9c, gr 20–15, gr 20–90) has porphyroclastic textures; the large olivine porphyroclasts are usually surrounded by mosaic aggregates of neoblastic, unstrained fine-grained olivine crystals. Orthopyroxene occurs as relics, like the rare clinopyroxene crystals, sometimes showing concentric zoning and very thin exsolution lamellae. Interstitial spinel is anhedral and does not exceed 1 mm. Lherzolite

Table 3
Representative major element (wt %) clinopyroxene compositions

Rock type	Wh	Wh	Hz	Hz	Hz	Hz	Hz	Hz	Hz	Hz	Hz	Lh	Lh	Lh	Lh	Du	Du	Wb	Wb	Wb	Lh	Lh
Sample	gr 7–1	gr 7–1	gr 20–22	gr 20–15a	gr 1–5	gr 1–2	gr 1–2	gr 5–1	gr 20–9c	gr 20–90	gr 20–15	gr 20–21	gr 20–15b	gr 20–2	gr 20–2	gr 7–2	gr 1	gr 20–10	gr 20–10	gr 20–13	gr 20–9a	gr 20–8
SiO_2	47.07	52.24	52.55	51.85	53.98	47.45	48.98	53.84	51.20	48.33	52.26	51.65	54.09	49.36	51.28	53.36	54.05	51.75	54.74	54.45	55.42	53.01
TiO_2	1.30	0.43	–	0.21	–	1.17	1.64	–	0.10	0.94	0.27	0.08	–	1.20	0.37	0.06	0.22	0.29	–	0.10	–	0.05
Al_2O_3	8.18	3.55	4.62	3.35	1.79	7.69	6.85	2.13	5.48	6.87	3.67	3.91	1.80	5.86	4.10	2.07	1.62	3.57	2.30	0.89	0.58	3.15
Cr_2O_3	0.14	0.64	0.65	–	0.95	0.46	–	1.04	2.26	0.77	0.76	1.76	0.83	–	0.24	0.90	0.05	0.11	0.47	0.18	0.50	0.50
FeO_{tot}	6.86	4.54	3.09	7.33	3.68	6.24	9.80	3.16	3.22	4.70	3.83	3.40	2.64	9.52	4.69	3.52	4.07	6.27	3.70	4.48	3.13	3.40
NiO	0.01	0.02	–	–	–	–	–	0.03	–	–	–	0.36	–	–	–	–	–	–	–	–	0.12	0.01
MgO	12.32	15.35	15.50	14.96	18.11	13.41	10.79	18.07	16.01	13.68	15.57	16.38	16.21	12.97	15.06	17.22	16.43	15.48	15.97	17.70	19.03	17.70
CaO	23.43	23.17	22.33	21.59	20.29	22.63	20.57	21.35	21.18	22.99	23.84	21.97	24.08	21.01	23.49	22.03	22.81	22.06	22.57	21.96	20.80	21.15
Na_2O	0.12	0.06	0.49	0.31	0.41	0.24	0.81	0.42	0.44	0.05	0.21	0.40	0.06	0.30	0.12	0.35	0.30	0.21	0.03	0.37	0.11	0.27
K_2O	–	–	0.01	0.03	0.05	0.04	0.24	–	0.01	–	0.02	–	–	0.01	0.02	0.01	0.03	0.03	0.05	0.02	–	0.04
Sum	99.43	100.0	99.24	99.63	99.26	99.33	99.68	100.0	99.90	98.33	100.4	99.91	99.71	100.2	99.37	99.52	99.58	99.77	99.83	100.2	99.69	99.28
Mg#	0.76	0.86	0.90	0.78	0.90	0.79	0.66	0.91	0.90	0.84	0.88	0.90	0.92	0.71	0.85	0.90	0.88	0.81	0.88	0.88	0.92	0.90

– Below detection limits; Wh = wehrlite; Du = dunite; Hz = harzburgite; Lh = lherzolite; Wb = websterite; Py = pyroxenite.

Table 4
Representative major element (wt.%) compositions of spinel

Rock type	Wh	Wh	Du	Du	Hz	Hz	Hz	Hz	Hz	Hz	Hz	Hz	Hz	Lh	Lh	Lh	Lh	Wb	Wb	Lh	Lh
Sample	gr 7–1	gr 7–1	gr b	gr b	gr 1–2	gr 20–9c	gr 20–9c	gr 20–90	gr 5–1	gr 5–1	gr 20–15	gr 20–8a	gr 20–8a	gr 20–2	gr 20–15b	gr 20–15b	gr 20–21	gr 20–13	gr 20–10	gr 20–9a	20–8c
TiO_2	0.36	0.58	0.16	0.36	0.92	0.06	0.08	0.15	–	0.03	0.63	0.20	0.15	0.02	0.20	0.14	0.10	0.06	0.28	–	0.34
$Al2O_3$	21.42	20.58	38.39	27.87	17.24	23.35	24.92	47.27	36.82	20.61	21.75	29.10	53.84	23.88	23.06	18.84	15.40	39.03	18.85	12.16	25.02
Cr_2O_3	44.29	29.95	21.09	33.84	40.07	40.80	22.23	15.04	27.71	46.49	38.80	36.00	14.34	38.56	40.89	42.71	49.69	25.25	39.15	51.82	35.34
FeO_{tot}	18.37	36.70	23.7	22.06	31.24	21.01	39.30	21.43	18.50	17.01	25.17	21.96	12.40	23.41	20.51	23.58	20.77	21.04	30.73	24.25	29.28
MnO	0.29	0.44	–	0.04	0.35	0.30	0.30	0.11	0.18	0.33	0.36	0.27	0.11	–	0.31	0.26	0.31	0.17	–	–	0.31
NiO	0.31	0.12	0.24	0.1	–	0.14	0.23	0.16	0.41	0.08	0.28	0.12	0.29	0.12	0.31	0.20	0.22	0.21	0.02	0.06	0.09
MgO	15.12	10.05	16.01	14.43	10.40	15.32	13.58	17.20	17.36	14.53	12.43	13.25	18.87	12.29	14.59	12.58	14.30	14.30	9.78	11.18	10.09
CaO	0.01	0.11	0.02	0.02	0.19	0.01	–	–	–	–	–	–	0.01	0.32	0.05	0.01	–	–	0.08	0.02	0.03
Na_2O	–	–	–	0.03	0.33	–	–	–	–	–	–	–	0.01	–	–	–	–	0.01	–	–	–
K_2O	–	–	0.03	0.04	0.09	0.03	0.05	0.04	–	–	0.02	0.05	0.01	0.03	0.01	0.02	0.02	0.02	0.10	0.02	0.03
Zn	–	–	0.14	0.03	–	0.02	0.01	0.06	–	–	0.04	–	0.08	–	0.23	0.17	0.13	0.13	–	–	–
Sum	100.2	98.53	99.77	99.15	100.7	101.0	100.7	101.5	101.0	99.00	99.48	101.0	100.1	99.08	100.2	98.52	99.95	100.2	99.61	99.60	100.5

– Below detection limits; Wh = wehrlite; Du = dunite; Hz = harzburgite; Lh = lherzolite; Wb = websterite; Py = pyroxenite.

(samples gr 20–21, gr 20–15b, gr 20–2, 20–9a) has porphyroclastic to granular textures. In granular samples, olivine (up to 3 mm) is almost unstrained and has only rare fractures. Dunite (samples gr 7–2, gr 1, gr 20b) is characterised by granular textures with medium-size crystals up to 2 mm. Olivine forms coarse rounded to euhedral grains with fractures and dislocation walls, displaying curvilinear to polygonal boundaries against adjacent olivine crystals. Anhedral spinels are sub-millimetre in size.

Infiltration of host basalts through the majority of peridotite samples is clearly documented by the presence of glass veins and melt pockets as the outer rim of the xenoliths is approached. Moreover, further evidence of interaction with the host basalt is provided by the presence toward the xenolith rim of fine-grained (sub-millimetric in size) aggregates of euhedral, secondary olivine, clinopyroxene and plagioclase crystals. The inner part of peridotite xenoliths also contains small melt pockets and a secondary mineral assemblage consisting of clinopyroxene, plagioclase, spinel and pargasitic amphibole. However, in the inner part of the xenoliths, melt pockets are insulated and a network of glass films and veins are not observed, suggesting that glasses document either an earlier in-situ melting or a metasomatic influx of fluids or melts before the uptake of xenoliths by host lavas. Textural evidence is confirmed by the chemical analyses of glasses (see below) which show a gap between basalt (glasses in the infiltrated portions of the outer xenoliths) and dacitic compositions (interstitial glass and glass pockets in the inner portions of the xenoliths).

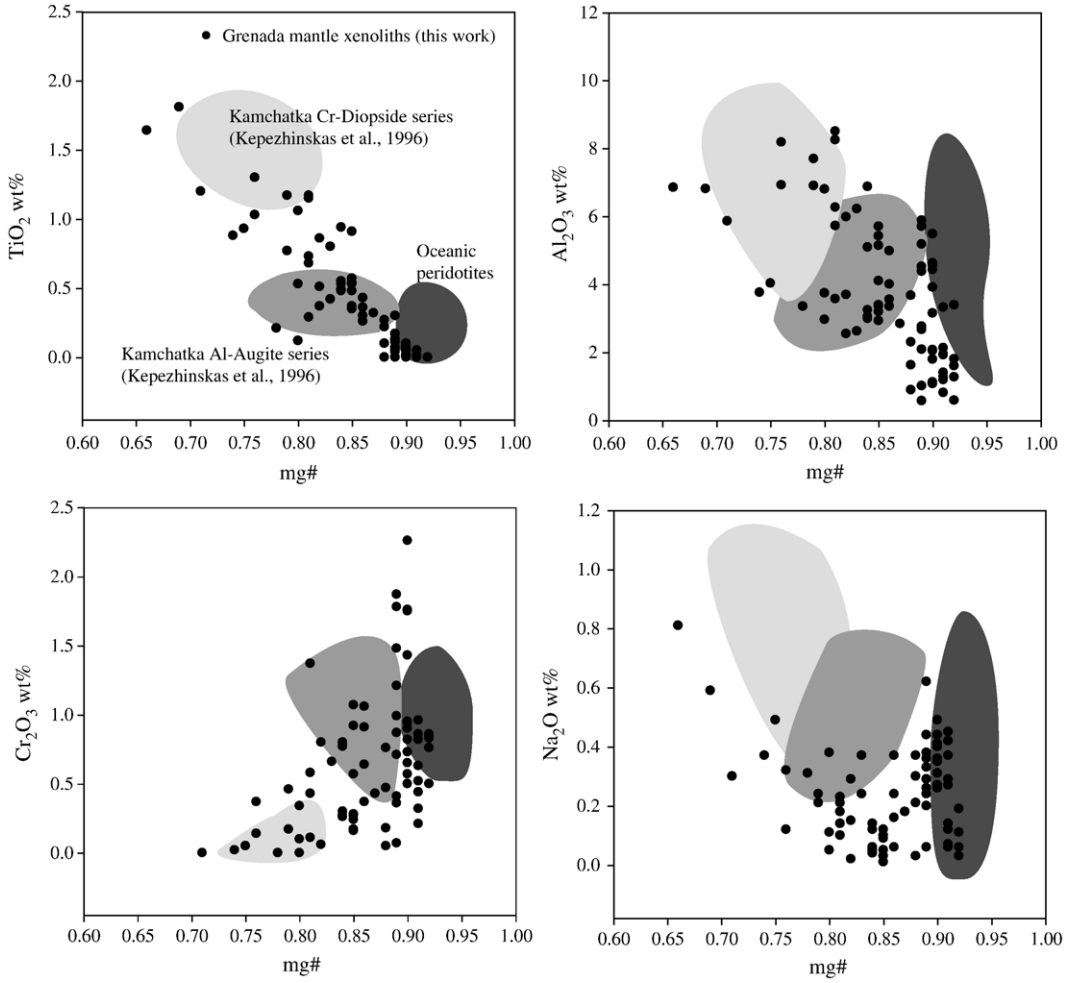


Fig. 1. TiO_2, Al_2O_3, Cr_2O_3 and Na_2O vs. Mg# in clinopyroxene. The fields of clinopyroxene from oceanic peridotites (Dick, 1989; Parkinson et al., 1992; Ishii et al., 1992) and from Kamchatka (Kepezhinskas et al., 1996) are reported for comparison.

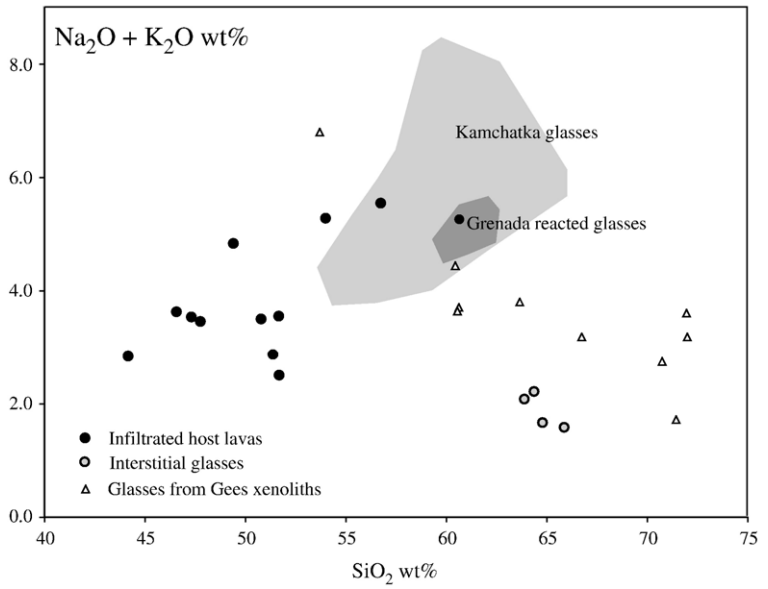


Fig. 2. Na_2O+K_2O vs. SiO_2 in glasses from Grenada xenoliths. The compositions of infiltrated host lavas and interstitial glasses are compared with those of reacted glasses from Parkinson et al. (2003) and of type II glasses from Gees xenoliths (Zinngrebe and Foley, 1995). The composition of glasses from Kamchatka mantle xenoliths (Kepezhinskas et al., 1996) is also shown.

Wehrlite has porphyroclastic textures with coarse (up to 2 mm) olivine and clinopyroxene and rare interstitial sub-millimetre spinel; most samples have been extensively infiltrated by the host lava and melt pockets are recognised also within porphyroclasts. Websterite and pyroxenite show granular textures; larger olivine and orthopyroxene (up to 3 mm) grains are highly deformed and crosscut by a network of closely spaced thin fractures filled by glass and secondary minerals as its crystallisation products.

4. Analytical methods

Mineral analyses of Grenada xenoliths were determined using the Camebax electron probe at the Institute of Volcanology and Geochemistry, Petropavlovsk-Kamchatsky, Kamchatka, Russia. Operating conditions were: a 20 kV accelerating voltage, a beam current of 15 nA, a counting time of 20 s and a beam diameter of approximately 2 μm. Glass analyses were obtained at the above conditions with a defocussed beam of 5 μm

Table 5
Representative major element (wt.%) compositions of glasses

Rock type	Du	Du	Du	Du	Hz	Hz	Hz	Hz	Hz	Hz	Hz	Hz	Hz	Hz	Wb	Lh
Sample	gr 7–2	gr 7–2	gr 1	gr 1	gr 1–5	gr 1–5	gr 1–5	gr 1–5	gr 20–15a	gr 20–15a	gr 1–2	gr 1–2	gr 1–2	gr 20–8a	gr 20–10	gr 20–2
SiO_2	44.16	46.56	51.65	53.99	63.96	64.27	65.85	64.78	51.67	51.37	47.73	47.45	50.78	60.64	56.73	49.40
TiO_2	1.02	1.19	2.11	1.91	0.20	0.23	0.21	0.26	1.64	1.61	2.47	2.49	1.94	0.34	1.96	2.22
Al_2O_3	20.18	17.59	16.35	18.03	17.47	17.34	17.58	17.06	15.97	15.88	14.13	13.94	13.67	22.01	22.54	15.89
Cr_2O_3	–	0.50	–	–	–	–	–	–	–	–	–	–	–	–	–	–
FeO	7.40	6.23	10.95	11.14	3.70	3.61	3.85	3.41	8.79	8.86	15.15	15.59	13.82	1.86	3.86	13.92
MnO	–	0.04	0.15	0.23	–	–	–	–	–	–	0.13	0.19	0.10	–	–	–
MgO	3.38	3.68	1.97	1.86	2.94	2.59	2.80	3.03	5.10	5.16	3.38	3.35	3.38	0.08	0.40	3.12
CaO	17.09	17.03	8.99	5.81	7.20	7.23	5.57	6.15	10.87	10.61	9.11	9.06	8.72	4.56	8.91	5.70
Na_2O	2.01	2.74	1.42	3.03	1.21	1.25	0.63	0.67	1.00	1.37	1.50	1.51	1.56	4.03	4.99	3.60
K_2O	0.84	0.89	2.13	2.25	0.90	0.95	0.96	1.00	1.51	1.51	1.97	2.01	1.94	1.23	0.56	1.24
Sum	96.08	96.45	95.72	98.25	97.58	97.47	97.45	96.36	96.55	96.37	95.57	95.59	95.91	94.75	99.95	95.09
Mg#	0.31	0.37	0.15	0.14	0.44	0.42	0.42	0.47	0.37	0.37	0.18	0.18	0.20	0.04	0.09	0.18

– Below detection limits; Wh = wehrlite; Du = dunite; Hz = harzburgite; Lh = lherzolite; Wb = websterite; Py = pyroxenite.

where possible, reducing counting time to <10 s. Some interstitial glasses have been analysed only with fully focussed beam due to their small size. Only minor alkali loss was suggested by the high totals of these analyses and the online observation of sodium count rates. A set of natural and synthetic standards was used; data reduction was based on the ZAF-correction procedure according to Bence and Albee (1968) and Albee and Ray (1970).

Trace elements were determined in-situ on thick polished sections using the LA-ICP-MS operating at the CNR-IGG in Pavia which couples a laser probe with an inductively-coupled plasma-mass spectrometer. The laser probe uses a pulsed Nd:YAG laser source "Brilliant" (Quantel, Les Ulis, France), whose fundamental emission in the infrared (1064 nm) is converted into 266 nm by means of two harmonic generators. For this work, the laser was operated at a repetition rate of 10 Hz, and the spot diameter was 20–40 μm with a pulse energy of about 0.1 mJ. The particles produced by ablation are then analysed by a field-sector mass spectrometer ("Element", Finnigan MAT, Bremen, Germany). Ablation signal integration intervals were selected by carefully inspecting the time-resolved analysis to ensure that no inclusions were present in the analysed volume, and data reduction was done by the software package "Glitter". NIST SRM 610 was used as the external standard, and ^{44}Ca was used as internal standard. Details are reported in Tiepolo et al. (2003).

5. Major-element mineral and glass chemistry

Primary olivine is $Fo_{88–93}$, whereas coexisting orthopyroxene is $En_{88–90}$ with generally low to very low-Al contents. Clinopyroxene has Mg numbers (Mg#) ranging from 85 to 92, with Al_2O_3 and Na_2O contents in the range 0.57–4 wt.% and 0.04–0.48 wt.%, respectively. Spinel is Cr-rich with Cr_2O_3 between 24.15 and 49.69 wt.% (representative analyses for selected samples are reported in

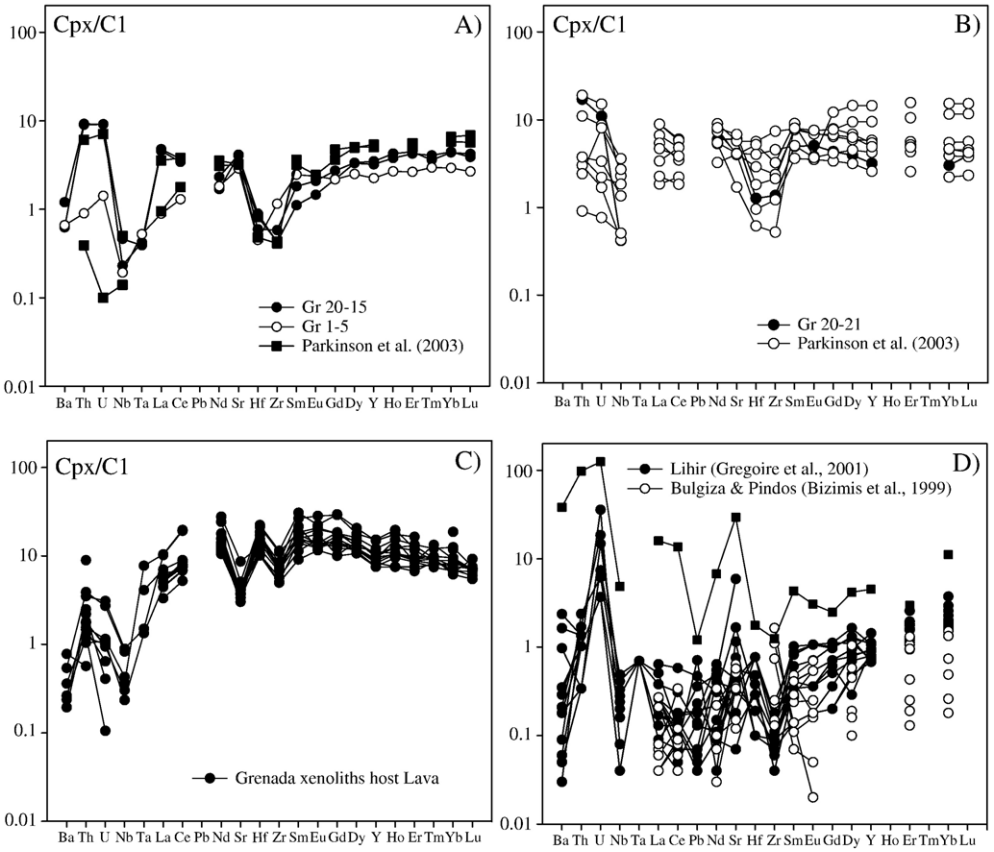


Fig. 3. Incompatible trace-element diagrams for clinopyroxenes from Grenada xenoliths: (A) primary mantle clinopyroxene; (B) reacted mantle clinopyroxene; (C) clinopyroxene crystallised from the host lava. In (D) the composition of clinopyroxene from other sub-arc mantle xenolith localities is reported for comparison. Values normalised to C1 chondrite (Anders and Ebihara, 1982).

Table 6
Clinopyroxene trace-element composition (ppm)

Sample	gr 1–2	gr 20–13	gr 20–13	gr 20–13	gr 20–21	gr 20–21	gr 20–2	gr 20–2	gr 20–10	gr 20–10	gr 20–90	gr 20–90	gr 20–15	gr 20–15	gr 1–5	gr 20–21
	Host lava	Host lava	Host lava	Host lava	Host lava	Host lava	Host lava	Host lava	Host lava	Host lava	Host lava	Host lava	Primary	Primary	Primary	Reacted
Sc	258	151	200	146	205	185	195	208	200	209	20.4	19.1	59.9	59.5	98	58.6
V	260	302	252	268	232	183	208	236	174	290	6.59	5.53	237	225	231	122
Cr	4738	1527	3377	3420	3042	1787	3681	4535	2157	4072	3.00	1.93	10,225	10,657	8680	7409
Rb	<1.273	<0.533	<0.424	<0.499	<0.325	<0.452	<0.384	<0.247	<1.216	<1.047	<1.215	<0.192	<0.528	1.090	<0.764	<0.369
Sr	33.3	29.8	28.5	31.6	29.8	26.3	33.0	28.7	23.6	31.7	8.64	5.10	32.2	31.4	22.5	47.1
Y	15.3	16.2	11.8	13.9	17.5	11.8	13.1	12.9	14.4	18.8	15.3	14.9	5.43	5.01	3.50	4.97
Zr	28.1	33.2	28.6	22.5	26.4	19.6	19.99	27.01	28.7	43.5	8.50	11.5	2.29	1.66	<1.153	5.41
Nb	0.203	0.105	0.057	<0.083	<0.092	<0.109	<0.115	0.074	<0.089	<0.186	0.890	0.366	0.057	0.113	0.047	0.103
Cs	<0.465	<0.201	<0.151	<0.181	<0.123	<0.177	<0.174	<0.174	<0.511	<0.495	<0.368	<0.258	<0.208	<0.326	<0.256	<0.254
Ba	1.26	<0.652	<0.404	0.841	<0.223	<0.490	0.615	0.454	1.820	<1.340	<1.120	<0.250	1.45	2.81	1.54	0.561
La	1.18	1.23	1.05	1.32	1.33	0.781	1.50	1.21	1.064	1.650	10.2	10.4	1.12	1.070	0.209	2.08
Ce	4.86	5.17	4.11	4.59	4.83	3.15	4.16	4.46	4.16	5.41	19.2	19.7	2.24	2.07	0.78	3.62
Pr	0.95	1.08	0.87	1.04	1.03	0.69	0.94	0.96	0.96	1.37	24.7	24.4	0.27	0.20	0.16	0.58
Nd	6.03	7.12	5.15	5.60	6.32	4.76	5.36	5.66	5.45	8.10	27.9	24.2	1.05	0.76	0.82	2.68
Sm	2.33	2.48	2.34	1.67	2.57	1.34	2.19	2.05	3.16	2.72	26.6	30.9	0.267	0.163	0.361	0.73
Eu	0.986	1.12	0.75	0.86	0.78	0.646	0.827	0.695	0.692	1.162	28.4	22.4	0.117	0.082	0.132	0.285
Gd	2.00	3.53	2.88	2.62	3.63	1.97	2.42	2.80	3.06	3.54	29.0	29.6	0.535	0.430	0.427	0.853
Tb	0.511	0.498	0.399	0.330	0.407	0.41	0.401	0.461	0.561	0.508	<4.16	<4.24	0.099	0.085	0.092	0.149
Dy	3.54	3.50	2.73	2.92	3.09	2.59	2.87	3.01	2.98	3.91	17.8	20.7	0.813	0.804	0.606	0.954
Ho	0.698	0.695	0.531	0.601	0.595	0.42	0.420	0.583	0.850	0.854	19.7	17.7	0.236	0.211	0.149	0.197
Er	2.08	1.83	1.36	1.39	1.54	1.07	1.20	1.40	1.36	2.14	12.1	16.4	0.709	0.675	0.420	0.797
Tm	0.227	0.215	0.180	0.225	0.24	0.21	0.193	0.199	0.323	0.293	<1.7	<1.8	0.087	0.098	0.072	0.07
Yb	1.01	1.45	1.10	1.05	1.55	1.14	1.35	1.24	1.50	2.04	11.9	18.7	0.711	0.724	0.475	0.491
Lu	0.133	0.167	0.163	0.225	0.172	0.15	0.175	0.175	0.168	0.183	<1.06	<1.68	0.103	0.094	0.065	0.096
Hf	1.94	1.78	1.63	1.08	1.26	1.05	1.12	1.49	1.77	2.22	13.0	22.4	0.062	0.093	0.047	0.132
Ta	<0.064	<0.023	0.019	<0.022	<0.021	<0.019	<0.079	<0.079	<0.052	0.058	1.50	7.75	0.006	0.006	0.007	<0.001
Pb	<0.451	<0.216	<0.167	<0.222	<0.273	<0.264	<0.301	<0.301	<0.538	<0.670	0.198	0.389	<0.258	<0.247	<0.289	0.158
Th	0.115	0.046	0.031	0.044	0.051	0.038	0.035	0.053	0.017	0.074	3.50	8.95	0.265	0.271	0.026	0.503
U	0.022	0.009	0.009	0.005	0.008	0.001	0.008	0.008	<0.001	<0.001	3.10	<0.001	0.074	0.074	0.011	0.089

Tables 1–4). These data are in excellent agreement with the data reported in the paper by Parkinson et al. (2003) to which the reader is referred to for a detailed presentation and discussion of mineral compositions.

In addition to the primary assemblage, secondary minerals (i.e., olivine, clinopyroxene and plagioclase) are observed in equilibrium with the infiltrating host basalt in the outer parts of the Grenada xenoliths. More rarely, a secondary metasomatic assemblage is observed in the inner parts of the xenoliths either within melt pockets or associated with interstitial glass. The metasomatic mineral assemblage includes Al-rich clinopyroxene (Al_2O_3 up to 8.2 wt.%, Na_2O up to 0.8 wt.%), plagioclase ($An_{45–80}$), Al-rich spinel (Al_2O_3 from 53 to 64 wt.%), and pargasitic amphibole. Unfortunately, the very small size of these minerals prevented trace-element investigations by LA-ICP-MS. We also ignored these mineral compositions to avoid unreliable data due to possible contamination from adjacent glass. In place of individual analyses, we selected areas of metasomatism for the in-situ determinations of trace elements with the aim of constraining the geochemical signature of the metasomatic agent.

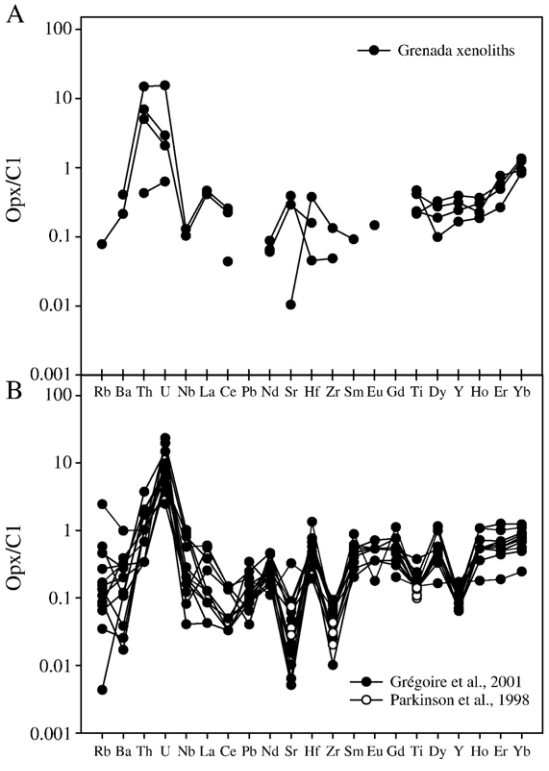


Fig. 4. (A) Incompatible trace-element diagrams for orthopyroxene from Grenada xenoliths; (B) orthopyroxene from other sub-arc mantle xenolith localities is reported for comparison. Values normalised to C1 chondrite (Anders and Ebihara, 1982).

Table 7
Orthopyroxene trace-element composition (ppm)

Sample	gr 20–13	gr 1–5	gr 20–15b	gr 20–2
Sc	14.7	34.0	27.9	8.08
V	18.5	144	102	13.4
Cr	830	6174	4670	519
Rb	<0.498	<0.637	0.180	<0.166
Sr	<0.201	2.27	3.05	0.081
Y	0.3	0.488	0.258	0.614
Zr	<0.746	<0.754	0.192	0.524
Nb	<0.048	0.032	0.025	<0.052
Cs	<0.244	<0.220	<0.048	<0.086
Ba	<0.429	0.951	0.501	<0.301
La	<0.033	0.109	0.096	<0.028
Ce	<0.023	0.155	0.135	<0.023
Pr	<0.008	<0.023	<0.012	<0.006
Nd	<0.046	<0.044	0.040	<0.052
Sm	<0.119	<0.135	<0.041	0.014
Eu	<0.083	<0.032	0.008	<0.014
Gd	<0.139	<0.150	<0.075	<0.122
Dy	0.04	<0.066	0.024	0.079
Ho	0.02	0.012	0.010	0.020
Er	0.07	0.121	0.042	0.091
Yb	0.15	0.149	0.135	0.220
Hf	<0.018	0.016	0.005	0.039
Ta	<0.011	<0.024	<0.009	<0.024
Pb	<0.271	<0.245	<0.097	<0.207
Th	0.013	0.437	0.204	0.148
U	0.003	0.125	0.024	0.017

As a whole, primary clinopyroxene is diopside and has Mg#, Ti, Al, and Na similar or slightly lower than those shown by clinopyroxene from oceanic peridotites (Fig. 1). In contrast, secondary clinopyroxene has progressively increasing Ti, Al, Na contents and decreasing Mg# values, trending towards the salitic clinopyroxene from host lavas which is characterised by the highest Al (up to 8.5 wt.%) and Na (up to 0.9 wt.%) contents. The compositional variation observed for secondary clinopyroxene from Grenada xenoliths is closely similar to that defined by clinopyroxene from Kamchatka xenoliths, which based on textural and chemical evidence has been interpreted as a reaction product between melt and sub-arc, host mantle peridotite (Kepezhinskas et al., 1996).

Glasses related to the infiltration of host lavas are basalt and andesite-basalt, whereas glasses from small veins and pockets show progressively higher silica and alkali contents (Fig. 2); interstitial glass from the inner part of the xenoliths is characterised by dacitic compositions and shows low Ti (0.2–0.34 wt.%), alkalies ($Na_2O+K_2O=1.5–2.2$ wt.%) and very high SiO_2 (up to 66 wt.%) and Al (up to 17.6 wt.%) contents (Table 5). Similar chemical compositions have been described by Zinngrebe and Foley (1995) for type II glass in mantle xenoliths from Gees (West Eifel, Germany).

Table 8
Trace-element composition of glasses related to the infiltration of host lavas (ppm)

Sample	gr 1–5	gr 1–5	gr 1–2	gr 1–2	gr 1–2	gr 1–2	gr 20–2	gr 20–2	gr 20–10	gr 20–15a	gr 20–15a	gr 20–15a
Sc	27.0	23.1	16.6	15.8	14.3	12.8	55.6	72.3	42.6	34.2	28.2	30.5
V	321	420	186	135	189	165	413	309	225	509	631	671
Cr	72.9	<11.4	<15.8	30.8	<11.4	<11.7	402	620	109	949	260	20,602
Rb	19.3	18.2	28.5	25.2	21.3	21.5	7.87	11.7	18.7	30.0	39.1	34.9
Sr	544	552	218	238	314	378	306	217	206	337	384	391
Y	19.6	23.8	11.3	8.98	11.6	10.5	31.9	25.2	19.8	31.0	37.3	39.3
Zr	67.6	89.1	67.0	63.2	62.7	60.0	133.	86.2	88.5	110	138	135
Nb	7.19	9.11	7.10	6.59	6.40	6.60	8.97	5.54	7.76	11.32	15.04	16.16
Cs	0.797	0.733	0.703	0.464	0.633	0.484	0.386	0.259	<0.37	1.16	<0.22	1.23
Ba	172	205	126	109	130	131	208	125	173	269	324	297
La	14.4	17.1	8.22	6.94	8.83	8.58	16.4	10.6	11.3	21.6	26.1	24.8
Ce	27.6	33.1	15.7	14.0	17.4	15.9	21.2	19.5	17.5	40.7	49.8	49.0
Pr	3.50	4.20	1.90	1.59	2.03	1.94	5.00	3.40	2.64	5.74	6.25	6.2
Nd	14.1	17.7	8.34	6.87	8.85	8.82	22.8	17.8	13.6	24.0	27.8	30.7
Sm	3.58	4.37	2.52	1.88	1.89	1.69	6.12	4.14	3.20	5.81	7.32	9.14
Eu	1.15	1.34	0.665	0.490	0.633	0.848	2.01	1.35	1.23	1.802	2.101	2.26
Gd	2.98	4.04	2.25	1.70	2.10	1.95	6.83	5.01	3.28	5.03	8.29	7.02
Dy	3.62	4.64	1.80	1.54	2.41	2.14	5.84	4.71	3.51	6.67	6.91	7.05
Ho	0.803	0.933	0.405	0.307	0.390	0.455	1.11	0.909	0.697	1.35	1.57	1.26
Er	2.28	2.58	1.04	1.05	1.22	1.14	3.27	2.51	2.07	2.83	4.04	5.81
Yb	2.24	2.39	1.01	1.12	1.47	1.37	3.42	2.44	1.58	4.1	4.75	4.28
Hf	1.72	2.26	1.61	1.58	1.78	1.77	4.04	2.87	3.23	3.33	2.88	3.15
Ta	0.396	0.520	0.343	0.349	0.383	0.306	0.607	0.309	0.383	0.729	0.855	0.808
Pb	4.40	2.97	4.99	3.73	3.68	3.57	3.81	2.57	4.08	1.85	3.37	1.45
Th	3.81	4.75	2.18	1.82	2.31	2.26	5.59	2.76	3.25	7.48	7.65	6.73
U	1.28	1.71	0.918	0.779	0.916	1.09	0.480	0.513	0.796	3.09	3.27	3.14

Due to the obvious limitations of pressure estimates for the spinel stability field, only temperature has been estimated for the primary mineral assemblages using commonly applied geothermometers (Wood and Banno, 1973; Wells, 1977; Brey and Köhler, 1990). The highest *T* values are recorded in websterites and lherzolites (1100–1200 °C), whereas harzburgites do not exceed 1050 °C. Although slightly higher, these temperatures are consistent with those calculated by Parkinson et al. (2003) for primary mantle clino- and orthopyroxene (850–925 °C) and the reacted rims of primary clinopyroxene and wehrlitic clinopyroxene (1070–1160 °C).

6. Trace-element composition of pyroxenes and glasses

Primary clinopyroxene (Fig. 3A; Table 6) is low in REE with chondrite-normalised abundances ranging from 1 to 5. The REE patterns are characterised by a shallow downward slope from HREE to LREE, negative HFSE and positive Sr anomalies. Selective La and Ce enrichment may occasionally occur, coupled with marked Th and U enrichments (U_N/Th_N close to unity). Two primary clinopyroxene grains analysed by Parkinson et al. (2003) show HREE abundances exceeding 10×C1, but their overall enrichment in highly incompatible elements, including Nb, suggests that they reacted at some extent with incoming melts (see reacted clinopyroxene below). The REE patterns of clinopyroxene which shows evidence, based on petrography or major element chemistry, of progressive reaction with metasomatic agents or host lavas show higher MREE abundances with negative fractionation from Sm to Lu. This clinopyroxene is characterised by variable LILE and LREE enrichment and negative HFSE anomalies (Fig. 3B).

Grenada clinopyroxene differs significantly from mantle clinopyroxene sampled in sub-arc mantle occurrences elsewhere (Fig. 3D). Clinopyroxene from oceanic sub-arc mantle is usually characterised by lower REE contents and steep downward REE spectra from HREE to LREE. In addition they usually show a strong fractionation of U relative to Th. This is the case of clinopyroxene from Lihir, Papua New Guinea (Grégoire et al., 2001) and Izu–Bonin peridotites (Parkinson and Pearce, 1998). Similar REE signatures are also observed in clinopyroxene from ophiolitic peridotites which is believed to represent fossil remnants of mantle wedge, (e.g., Bay of Island, Batanova

gr 20–15a	gr 20–15a	gr 20–15a	gr 20–15a	gr 20–15a	gr 1–5	gr 1–5	gr 1–5	gr 1–5	gr 1–5	gr 1–5	gr 1–5	gr 1–5
36.7	32.2	31.9	33.8	37.3	32.0	36.1	39.9	32.2	40.3	38.7	47.0	37.6
515	427	486	551	441	480	272	272	234	287	258	248	347
201	142	164	174	160	208	104	108	392	111	79.7	94.0	14.9
32.3	29.4	34.5	36.9	20.8	18.9	20.4	17.8	12.2	24.7	18.2	16.6	20.6
396	363	353	393	386	204	244	241	157	293	240	231	250
39.8	34.4	31.8	35.2	24.8	5.12	7.47	7.04	4.38	7.19	6.97	7.05	7.7
151	114	116	131	88.4	6.64	9.86	9.40	4.89	6.62	7.25	4.93	14.2
14.97	10.78	12.08	13.82	9.73	0.703	1.82	1.43	0.777	1.51	1.11	1.20	1.05
1.61	1.97	1.65	2.03	<0.27	0.300	0.637	0.496	0.435	0.536	0.68	0.84	<0.27
333	300	303	318	193	72.4	128	117	92.3	114	103	89.5	113
27.2	22.7	23.4	25.1	17.2	2.36	2.74	4.38	3.94	3.9	4.63	3.74	4.21
53.0	48.9	45.3	48.3	32.0	5.34	10.07	9.33	6.94	5.31	6	8.23	12.03
6.2	6.09	5.27	5.45	3.73	0.569	1.082	0.939	0.637	0.784	0.568	0.717	0.958
31.3	24.7	24.4	26.2	20.6	1.7	3.64	3.8	3.12	3.09	3.93	3.05	3.07
6.94	5.11	6.15	6.61	4.52	0.84	0.278	0.941	0.53	0.578	0.45	0.639	0.58
1.78	2.17	1.83	2.02	1.81	0.259	0.189	0.454	0.149	0.29	0.53	0.172	0.232
6.87	6.91	6.04	5.45	4.17	0.51	0.9	0.838	0.682	0.443	0.47	0.49	0.69
7.71	7.63	6.61	6.8	5.06	1.40	1.79	1.12	0.446	1.05	1.12	1.02	0.78
1.37	1.32	1.19	1.38	0.803	0.207	0.131	0.347	0.195	0.218	0.353	0.466	0.414
4.76	3.94	3.39	3.94	2.37	0.45	1.38	1.11	0.627	0.767	0.306	0.474	0.58
4.31	3.38	3.28	4.05	3.76	0.600	0.94	1.23	0.279	1.51	0.84	1.81	1.13
3.93	2.92	2.53	3.52	3.24	<0.023	0.131	0.139	0.196	0.228	<0.041	0.184	<0.65
0.811	0.764	0.618	0.762	0.381	0.184	0.051	0.099	0.043	0.044	<0.019	<0.018	0.147
7.88	6.55	6.35	7.41	5.65	1.33	3.56	2.53	2.97	3.35	1.56	2.98	4.13
8.09	6.44	5.84	7.51	4.8	0.655	3.09	2.52	2.69	3.43	3.12	2.87	1.85
3.52	2.33	2.42	3.09	2.09	0.728	1.10	1.07	2.26	1.22	0.952	1.01	1.02

et al., 1998; and Hellenic Peninsula, Bizimis et al., 2000). Primary Cr-rich clinopyroxene from the Kamchatka arc mantle shows contrasting compositions. It is more enriched in REE, with MREE exceeding 10 times C1 chondrite and convex-upward patterns (Kepezhinskas et al., 1996), thus testifying to higher degrees of interaction with metasomatic agents which overprinted the original chemical signatures after partial melting.

Clinopyroxene in equilibrium with infiltrating host lavas is markedly different from both primary and reacted clinopyroxenes, although they share with these latter Gd_N/Yb_N values higher than unity. Clinopyroxene from host lavas (Fig. 3C) exhibits LREE-depleted ($La_N/Sm_N \sim 0.35$) convex-upward patterns with MREE up to 30×C1 and Gd_N/Yb_N fractionation up to 1.8; moreover, they are slightly depleted in Nb, Sr, and Zr and have positive Th and U anomalies. The overall geochemical signature of this clinopyroxenes is that expected from phenocrysts crystallised from basaltic to andesitic melts. In fact, the clinopyroxene can be related to the original host magma through a set of partition coefficients approaching those experimentally determined for corresponding system compositions (e.g., Hart and Dunn, 1993).

The REE patterns for orthopyroxene (Fig. 4A; Table 7) have marked downward slopes from HREE (0.8–1.3×C1) to MREE (0.2–0.5×C1), with a concave up-trend to LREE (0.4×C1). The incompatibility diagrams are characterised by large positive U and Th spikes (element concentration up to 15×C1) and in the LREE-enriched orthopyroxene, a small, but significant, positive Sr anomaly occasionally occurs. In general, Grenada orthopyroxene compares well with orthopyroxene from Izu–Bonin (Parkinson and Pearce, 1998) and Papua New Guinea (Grégoire et al., 2001) peridotites (Fig. 4B). However, a more detailed observation of the extended trace-element spectra for the latter reveal negative Ba, Sr, Zr, and Ti anomalies and positive spikes in U, but not in Th.

Glasses formed by infiltration of host lavas (Table 8) are LREE-enriched with smoothly fractionated REE patterns from LREE (La ranges from 29 to 115×C1) to HREE (Yb ranges from 6.2 to 21×C1) and La_N/Yb_N values ranging from 4 to 5. Incompatibility diagrams (Fig. 5A) display negative Nb and Ta anomalies (which nevertheless are lower than those usually shown by common IAB lavas), Nb/Ta normalised values around unity, and only slightly negative Zr and Hf anomalies. U

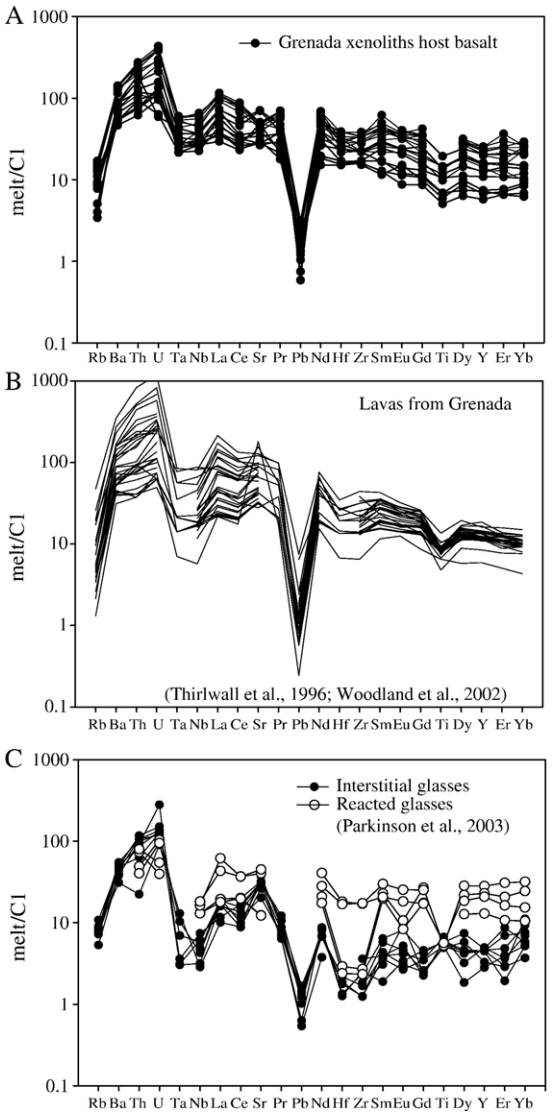


Fig. 5. Incompatible trace-element diagrams for infiltrated host lavas (A) and interstitial dacitic glasses (C) in Grenada xenoliths. The composition of reacted glasses from Parkinson et al. (2003) is also shown. The composition of the different Grenada magma series is reported for comparison (B). Data are from Thirlwall et al. (1996) and Woodland et al. (2002). Values normalised to C1 chondrite (Anders and Ebihara, 1982).

and Th exhibit large positive anomalies with C1-normalised values exceeding 400, whereas Pb is strongly depleted ($0.3 \div 3.2 \times$C1). Marked positive Sr anomalies are often observed. In general, the glass compositions determined by LA-ICP-MS in the infiltrated parts of the xenoliths cover the entire compositional range defined by Grenada lavas pertaining to the M- and C-series, to the M–C transitional series and to the high-SiO_2 andesites (Fig. 5B).

Interstitial glass and glass pockets of dacitic composition from the inner part of the xenoliths (Fig. 5C; Table 9) are characterised by significantly lower trace-element abundance (La up to $19 \times$C1) and different incompatibility diagrams. They exhibit marked negative HFSE anomalies with Nb_N/Ta_N around 0.5, large positive Sr anomalies and positively fractionated REE patterns from MREE to HREE ($Gd_N/Yb_N \sim 0.58$). The critical ratios between geochemically important elements (i.e., $Sr/Y = 32 \div 40$ and $La/Yb = 1.4 \div 3.8$) along with Cr contents up to 400 ppm are intermediate between those of classical island-arc lavas and those of adakites.

7. Discussion

7.1. Nature of the pre-metasomatic mantle

Textural and chemical evidence clearly shows that the Grenada xenoliths represent a sampling of the lithospheric mantle beneath the island, and that this mantle section underwent a chemical re-fertilisation as a consequence of metasomatic processes probably via melts and/or fluids formed in a subduction environment. This is in agreement with the conclusions of Parkinson et al. (2003). It is well accepted that Grenada is a volcanic island related to the subduction of the Atlantic Ocean beneath the Caribbean Plate. Accordingly, the sampled mantle xenoliths should represent fragments of pristine oceanic mantle which presently forms the mantle wedge overlying the subducting plate. This interpretation is confirmed by the close match of major element composition of clinopyroxene from Grenada xenoliths with that of clinopyroxene from oceanic environments (Dick, 1989; Parkinson et al., 1992; Ishii et al., 1992; Fig. 1).

The major element chemical composition of the most Mg-rich (primitive) pyroxene suggests the oceanic mantle was variably depleted as a consequence of partial melting and melt removal before the re-fertilisation operated by metasomatic agents rising from the underlying subducted slab. Unfortunately, trace elements allow only a rough evaluation of the extent of partial melting events. Even the most primary (i.e., less reacted) clinopyroxene underwent a slight re-fertilisation as evidenced by the LREE, MREE and, possibly, Sr values in the incompatibility diagrams of Fig. 3A. Thus, the degree of partial melting can be better inferred from the HREE composition because these elements are considered poorly affected by partial melting and metasomatic processes (Hellebrand et al., 2001). Assuming a depleted mantle as a starting composition and the melting model proposed by Johnson (1990), the

Table 9
Representative trace-element composition of interstitial glasses (ppm)

Sample	gr 1–5	gr 1–5	gr 1–5	gr 1–5	gr 20–90	gr 20–90	gr 20–90	gr 20–90
Sc	31.98	36.12	39.91	32.15	40.27	38.69	46.96	37.59
V	480	272	272	234	287	258	248	347
Cr	208	104	108	392	111	79.7	94.0	14.9
Rb	18.9	20.4	17.8	12.2	24.7	18.2	16.6	20.6
Sr	204	244	241	157	293	240	231	250
Y	5.12	7.47	7.04	4.38	7.19	6.97	7.05	7.7
Zr	6.64	9.86	9.40	4.89	6.62	7.25	4.93	14.2
Nb	0.703	1.82	1.43	0.777	1.51	1.11	1.20	1.05
Cs	0.300	0.637	0.496	0.435	0.536	0.68	0.84	<0.27
Ba	72.4	128	117	92.3	114	103	89.5	113
La	2.36	2.74	4.38	3.94	3.9	4.63	3.74	4.21
Ce	5.34	10.07	9.33	6.94	5.31	6.00	8.23	12.03
Pr	0.569	1.082	0.939	0.637	0.784	0.568	0.717	0.958
Nd	1.7	3.64	3.8	3.12	3.09	3.93	3.05	3.07
Sm	0.84	0.278	0.941	0.53	0.578	0.45	0.639	0.58
Eu	0.259	0.189	0.454	0.149	0.29	0.53	0.172	0.232
Gd	0.51	0.9	0.838	0.682	0.443	0.47	0.49	0.69
Dy	1.40	1.79	1.12	0.446	1.05	1.12	1.02	0.78
Ho	0.207	0.131	0.347	0.195	0.218	0.353	0.466	0.414
Er	0.45	1.38	1.11	0.627	0.767	0.306	0.474	0.58
Yb	0.600	0.94	1.23	0.279	1.51	0.84	1.81	1.13
Hf	<0.023	0.131	0.139	0.196	0.228	<0.041	0.184	<0.65
Ta	0.184	0.051	0.099	0.043	0.044	<0.019	<0.018	0.147
Pb	1.33	3.56	2.53	2.97	3.35	1.56	2.98	4.13
Th	0.655	3.09	2.52	2.69	3.43	3.12	2.87	1.85
U	0.728	1.10	1.07	2.26	1.22	0.952	1.01	1.02

HREE composition of clinopyroxenes from Grenada xenoliths can be achieved with about 18% partial melting, in good agreement with previous estimates by Parkinson et al. (2003) based on both clinopyroxene (~18–22%) and orthopyroxene (~20%). The predicted partial melting amounts are typical of clinopyroxene from oceanic and sub-arc environments and similar to the estimates for the clinopyroxene of the Bay of Island ophiolites complex (Batanova et al., 1998) and Lihir (Papua New Guinea; Grégoire et al., 2001).

Based on their mineral assemblage and chemistry, Grenada xenoliths appear to be brought up from the shallow mantle near the crust–mantle boundary (~30–50 km) and therefore they not likely represent fragments of peridotites at the bottom of the mantle wedge or from source regions of present arc magmas. Other lines of evidence (Parkinson et al., 2003) suggest that Grenada harzburgites are residual to melting within a pre-lesser Antilles subduction zone, rather than in an advecting asthenospheric mantle. On this basis, it seems highly probable that the xenolith lithologies underwent repeated episodes of metasomatism by either slab-related fluids and/or fractionated melts produced by differentiation of basaltic and andesitic liquids on their way to the surface.

7.2. Re-fertilisation of the refractory mantle wedge

Previous studies concluded the dominant reaction between melts and ambient peridotite mantle recorded at Grenada is the generation of wehrlite at the expense of orthopyroxene (Parkinson et al., 2003). This process resulted from the interaction of low-Si melts (similar to host M-series magma) which re-fertilised sub-arc mantle leading to a clinopyroxene-rich lithologies. However, this kind of process is not the only one the Grenada xenoliths underwent during their evolutionary stages and actually record. Three points need to be carefully addressed:

1) The trace-element chemistry of glasses in the infiltrated parts of the xenoliths is not compatible with reactive melt percolation processes operated by a single parental melt progressively evolving in composition. The glasses span the entire compositional range of Grenada lavas, i.e., from most primitive M-series, through C- and M–C-series to the high-SiO_2 andesites, showing almost parallel incompatibility patterns. The absence of fractionation among element with different incompatibility is in contrast with the compositional gradients expected

to be formed by infiltration of picritic/basaltic magmas and their reaction with the overlying mantle column under variable melt/rock volumes.

2) If harzburgite represents the sub-arc refractory mantle that has been only partially re-fertilised by the migration of arc magmas after large degrees of partial melting, then lherzolite should be regarded as intermediate products of progressive melt/mantle interaction (i.e., significantly re-fertilised) before the wehrlite formation. On this ground, clinopyroxene from harzburgite should possess, relative to their analogues from lherzolite, more fractionated spectra with pronounced LILE and LREE enrichments with respect to more compatible elements (Bodinier et al., 1990; Bedini et al., 1997). This difference is not observed in Grenada clinopyroxene which exhibits significant variations only in the most incompatible elements regardless of their occurrence in lherzolite and harzburgite samples.
3) The metasomatic signatures of Grenada pyroxene which are unaffected by metasomatism or poorly reacted with host lavas show close similarities with the trace-element composition of dacitic melts found in veins and pockets within mantle xenoliths. In particular, a good correspondence is found for the key elements U, Th, LREE, and Sr.

The chemical effects on the primary mineral assemblage of Grenada xenoliths related to the infiltration of the metasomatic agent can be evaluated on the basis of the differences between the trace-element signature of the most reacted pyroxene and those preserving the most primary composition. From the incompatible trace-element diagrams of Figs. 3A and 4A, it is evident that more reacted clinopyroxene and orthopyroxene are characterised by strong LREE, U, and Th enrichment compared with the primary and less reacted ones. This LREE, U and Th overprint is attributable to the interaction of a metasomatic agent that was extremely rich in these elements. Apparently, Sr does not appear to have been modified by the metasomatic process, since the majority of primary and reacted pyroxene shows a positive (and quite constant) Sr anomaly, that is not present in clinopyroxene in equilibrium with host lava. Since a positive Sr anomaly is not a common feature of refractory pyroxene after extensive partial melting degrees of oceanic peridotites, and given that LILE and most incompatible LREE react faster than Sr during reactive porous flow and are more efficiently transported by evolved melts/fluids, two alternative interpretations can be made: 1) none of the investigated pyroxene records pristine (i.e., refractory) Sr compositions, possibly because most primary minerals found in Grenada xenoliths were already slightly fluxed by an earlier metasomatic agent before the LREE, U and Th addition; 2) Sr enrichment is a primary feature of refractory mantle clinopyroxenes due to fluid-assisted melting of mantle sectors fluxed by slab-derived fluids. Noticeably, both hypotheses require the presence of Sr-enriched agents; moreover, the Sr enrichment, although at variable extent, is a common feature of Grenada lavas and interstitial glasses within mantle xenoliths.

The textural and chemical evidence that Grenada xenoliths reacted before and during their ascent to the surface with melts similar in compositions to the host lavas might lead to the conclusion that these latter caused the metasomatic overprint. However, different lines of reasoning lead us to consider unlikely that the LILE and Th, U enrichments observed in primary and reacted clinopyroxenes are entirely related to the interaction with host lavas. The first argument against this interpretation is that the clinopyroxene in equilibrium with the host lava is not enriched in LREE relative to HREE, has U and Th values more than two times lower than metasomatic clinopyroxenes, and a negative Sr anomaly. This geochemical signature is markedly different from that of spatially associated clinopyroxene which records the highest metasomatic enrichment. According to the more recent models describing the chemical effects of melt percolation (Vernières et al., 1997; Bedini et al., 1997; Xu et al., 1998), large volumes of percolating melt, such as those observed in the outer parts of the xenoliths, basically result in completely re-equilibrated pyroxenes which are related to the melt by sets of reliable partition coefficients. This is the case of clinopyroxene in Fig. 4C. Alternatively, small volumes of fractionated melts evolved from the host lavas can produce selective enrichments in most incompatible elements, and this metasomatic signature could have survived (based on kinetic reasons) the late arrival of larger volumes of melts preceding the uptake of the xenoliths. Quite apart from the problem that this process does not result in Sr enrichments relative to the adjacent LREE, a chromatographic separation of trace elements through host peridotite during melt percolation is expected to produce different patterns in lherzolite and harzburgite samples in light of their different porosities (i.e., melt/peridotite volume ratio) and of their different bulk distribution coefficients (Navon and Stolper, 1987; Bodinier et al., 1990; Vernières et al., 1997). Similar chemical gradients of LILE and LREE over more compatible elements depending on the rock composition (i.e., harzburgite vs. lherzolite) and textural position are not observed in Grenada pyroxenes, which therefore

cannot be simply regarded as refractory phases re-fertilised by interaction with host lavas.

A further and stronger evidence in favour of an earlier metasomatic agent unlike the host lavas is the strong parallelism between the metasomatic signatures of Grenada pyroxene and the trace-element composition of dacitic melts found in veins and pockets within mantle xenoliths (Fig. 5C). The good correspondence found for the key elements U, Th, LREE and Sr suggests a strong genetic relationship and points to a common metasomatic agent that either reacted with the mantle wedge beneath Grenada or was re-mobilised by later melting of a previously enriched mineral assemblages. In the former hypothesis, interstitial glasses are regarded as remnants (possibly highly reacted) of infiltrated metasomatic agents, whereas in the latter dacitic glasses formed by in-situ melting of a LILE-enriched mineral assemblage with a subordinate contribution of percolating melts similar to host lavas.

7.3. The origin of dacitic melts

The origin of silica-rich interstitial glasses is crucial to reconstruct the metasomatic history of the mantle column beneath Grenada. Do dacitic melts represent relics of earlier metasomatic agents, completely unlike the host lavas or did they formed as end products of melt/mantle reaction processes operated by melts similar to host magmas? None of these hypotheses are regarded as plausible.

Based on their compositions, it could be argued that dacitic glasses are comparable to adakites, and not typical arc melts (Kepezhinskas et al., 2000). This view could be supported by the occurrence of adakites on Grenada (Defant et al., 2000) and the analogy with the geologic setting and the metasomatic signatures of Kamchatka xenoliths (Kepezhinskas et al., 1995, 1996) which document island-arc metasomatism by peridotite-slab melt interaction. As for major elements, dacitic glasses share some similarities (namely SiO_2 and Al_2O_3 content) with adakite lavas from the Andean Austral Volcanic Zone (Stern and Kilian, 1996) and Kamchatka (Kepezhinskas et al., 1996). However, they have low-Na_2O content and do not completely match the composition of surface lavas in some parameters such as the Mg#, the alkali (Na_2O; K_2O) and the TiO_2 content. Moreover, quite apart some overall similarity with natural occurring transitional adakites (e.g., Kamchatka and AVZ) and with the experimental transitional adakite from Rapp et al. (1999), dacitic glasses are characterised by deep negative Zr and Hf anomalies and possess higher HREE, Ba/Zr (8–19), Nb/Zr (up to 0.24) and lower Sr/Y (≤ 40) with respect to adakite-type lavas (Fig. 6). Thus, chemical evidence indicates that the composition of the interstitial glass and glass pockets of dacitic composition from the inner part of the xenoliths is not that of adakitic composition. That is, it is distinctly different from the adakite glasses described in other mantle xenolith occurrences, such as from Kamchatka and the Philippines (Defant and Kepezhinskas, 2001).

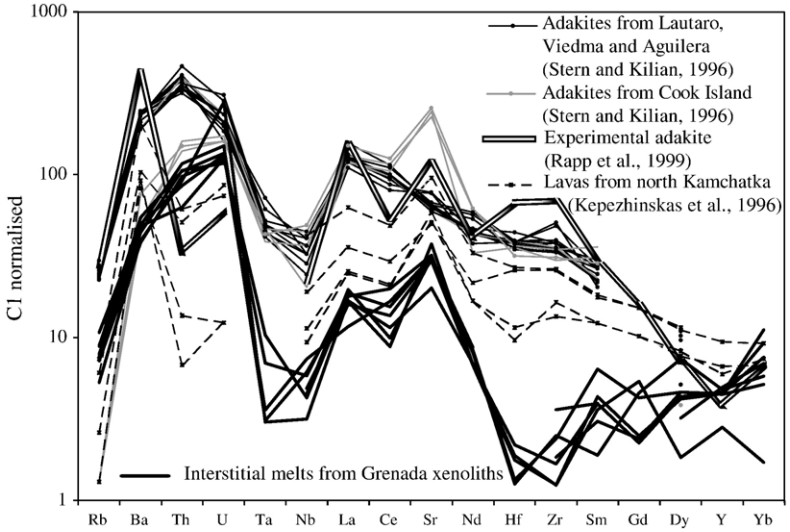


Fig. 6. Incompatible trace-element diagram comparing dacitic melts from Grenada xenoliths with natural and experimentally-produced adakites. Values normalised to C1 chondrite (Anders and Ebihara, 1982).

Those glasses show the typical HREE and Y depletions of adakites not found in the Grenada xenolith glasses.

Geological reasons may also explain the lack of adakite fingerprinting within shallow lithospheric mantle. Parental melts of adakites should originate at pressure equivalents at >120 km depth, i.e., in the subducted slab or in the lowermost mantle wedge. It seems thus plausible that these melts may have not survived percolation through at least 70–90 km of mantle wedge peridotites before reaching (unmodified or poorly modified) the shallow peridotites (30–50 km depths), now outcropping as basalt-borne xenoliths.

Alternatively, high-silica glasses could be regarded as the end products of melt/mantle reaction processes generated by melts similar to host magmas. These reactions have been described in other mantle xenolith occurrences (Zinngrebe and Foley, 1995) and reported for Grenada xenoliths by Parkinson et al. (2003). They lead to the generation of wehrlites at the expense of orthopyroxene and silica-rich melts.

Glasses reported by Parkinson et al. (2003) fall at the end of the alkali vs. SiO_2 trend (Fig. 2), clearly representing highly evolved compositions completely unlike dacitic glasses described in this work which are characterised by higher silica and much lower alkali contents. Dacitic glasses also differ from reaction glasses for their lower Nb, Ta and L-MREE contents, the positive Sr anomaly and a marked positive upward slope from MREE to HREE (Fig. 5C). In contrast, reaction glasses reported by Parkinson et al. (2003) show geochemical signatures still reminiscent of host lavas, in spite of the obvious fractionation induced by peridotite/melt reaction.

In terms of major elements, the interstitial glasses reported in this paper have some similarities, namely high silica and alumina contents and low alkalies, with type II glasses from Gees xenoliths (West Eifel, Germany, Zinngrebe and Foley, 1995). These glasses have been interpreted as derived by AFC-type reaction between basalt (opx-undersaturated) and harzburgite wall-rock. The pre-eruption melt composition, although extensively modified during ascent by dissolution of olivine and orthopyroxene and by crystallisation of microlites, was estimated to be a high-alumina basaltic andesite (55–60 wt.% SiO_2, 18 wt.% Al_2O_3, 2 wt.% alkalies). In Gees glasses the progressive reaction between percolating melt and peridotite minerals (mainly orthopyroxene) is documented by a progressive decrease of the alkali content with increasing silica (see Fig. 2). This is not observed for interstitial glasses from Grenada, which are clearly separated from reacted glasses (this work and Parkinson et al., 2003; Fig. 2) by a large compositional gap.

We agree that the observed gap can result from sample bias and that an origin of our interstitial glasses by reaction between incoming melt and ambient peridotite cannot be ruled out. However, textural evidence also indicates that interstitial glasses occur in the inner portions of the xenoliths without an apparent network of veins and are unrelated to frozen host lavas in the outer rim of xenoliths part. This, along with the absence of chemical gradients in both interstitial glasses and pyroxenes (usually observed during reactive porous flow or melt percolation through ambient peridotite; cfr. Bedini et al., 1997; Wulff-Pedersen et al., 1999) and the strong similarity with the geochemical signatures of associated pyroxenes, strongly suggests that dacitic glasses do represent the products of an in-situ melting caused by temperature increase before and during the uptake of xenoliths by host lavas. The refractory (harzburgitic) nature of sub-arc mantle accounts for the low alkali (and particularly Na) content of these melts, unlike evidence from natural and experimental melts from more fertile peridotite compositions (Baker et al., 1995; Hirschmann et al., 1998). In other words, we believe that dacitic glasses could be local re-melts of regions metasomatically enriched by earlier arc magmas that had stalled, fractionated, and solidified in the upper mantle. These local re-melts thus reflect the metasomatic component formed by earlier arc-related metasomatic agents and suitable to be re-mobilised by later melts during their migration towards the surface. This appears to be also the easiest way to explain the compositional similarities between the erupted arc lavas and the metasomatised peridotites.

8. Concluding remarks

Parkinson et al. (2003) documented that shallow sub-arc mantle beneath Grenada significantly interacted with percolating low-silica melts after older fractional melting events within a pre-lesser Antilles subduction zone. We provide here geochemical evidence that the geochemical signatures of Grenada xenoliths probably result from several stages of metasomatism, the last of which was most likely operated by uprising alkali basalts (M-series).

Inferences on the nature of metasomatic agents which re-fertilised the lithosphere mantle after the partial melting (but before the percolation of later alkaline melts) can be derived from the composition of primary and reacted pyroxene, and, more importantly, on the trace-element signatures of interstitial dacitic melts. The observed strong LREE, Ba, Sr, U and Th enrichment coupled with marked HFSE depletion are typical

features of fluids and magmas from arc-related settings. In normal subduction zones where thermal gradients are relatively low, the mantle wedge is fluxed by aqueous fluids released as a consequence of the slab dehydration. LILE are expected to possess the highest mobility in aqueous fluids (e.g., Keppler, 1996), and thus are the most suitable for the detection of the involvement of an aqueous agent in the metasomatic process. However, because pyroxene, due to structural impediments, cannot host Ba, Rb and the other large-ion elements, no useful information can be achieved from this group of elements. An exception is made for Sr, but this element does not give an unique answer on the nature of the slab flux because positive Sr anomalies, even if with different entities, are present in lavas originated from both partial melting of the subducted slab (adakites; e.g., Stern and Kilian, 1996) and partial melting of the mantle wedge fluxed by aqueous fluids (e.g., McCulloch and Gamble, 1991). The positive Sr anomaly shown by pyroxene thus would agree with either an aqueous or a silicate metasomatic agent. Even if the partitioning data show that LREE have a slightly higher compatibility than HREE, the REE group can be generally considered immobile in aqueous fluids (e.g., Brenan et al., 1995).

In Figs. 3D and 4B, the metasomatic signatures of mantle pyroxene from Grenada xenoliths are compared with those of pyroxene from arc settings, fluxed by aqueous fluid (Grégoire et al., 2001). The latter are depleted in LREE up to one order of magnitude relative to those of Grenada clinopyroxene and are characterised by an abrupt positive U anomaly and strong U/Th fractionation. According to experimental data (Brenan et al., 1995; Keppler, 1996), U has a significantly higher compatibility than Th in aqueous fluids that leads to U/Th fractionation during dehydration processes. On this basis, the metasomatic agent that fluxed the mantle wedge producing the strong LREE and Th enrichment, as well as the nearly chondritic U/Th value, in Grenada pyroxene was most likely a silicate melt and not a pure aqueous fluid.

This conclusion is consistent with recent experimental evidence for fluids and melts equilibrated with basaltic eclogite at depth conditions $\leq$ 120 km (Kessel et al., 2005). Whereas solubilities of Rb, Cs, Ba and Pb are high even in low-*T* aqueous fluids, only high-*T* (900 °C) aqueous fluids or hydrous melts (1000 °C) are efficient carriers of Sr, LREE, Th and U and thus plausible metasomatic agents for Grenada sub-arc mantle. Given that Grenada xenoliths do represent fragments of a shallow mantle near the crust–mantle boundary and not peridotites at the bottom of the mantle wedge which are more easily fluxed by slab-derived fluids, their metasomatic fingerprintings are more likely related to interaction with sub-arc melts. Geological and geochemical arguments suggest that these latter did not form by melting of subducted slab, but generated in the deeper (relative to the mantle level sampled by xenoliths) portion of the mantle wedge, fluxed by slab-derived fluids (Thirlwall et al., 1996).

The results of this study have two major implications. Firstly, pyroxene from Grenada xenoliths can be regarded as representative of pyroxene compositions in upper lithospheric mantle sectors which interacted with IAB melts. Accordingly, they can be used for comparative purposes in studies of mantle lithologies from back-arc regions which had their pristine (i.e., sub-arc) geochemical signatures overprinted by the percolation of large volumes of post-orogenic alkaline melts from deeper asthenospheric mantle regions, as it is the case of Southern Patagonia (Rivalenti et al., 2004).

Secondly, our results indicate that the lithospheric mantle beneath Grenada acquired its geochemical fingerprinting during the thickening of arc crust. Repeated episodes of peridotite interaction with earlier arc magmas that had stalled, fractionated, and solidified in the upper mantle led the mantle column to possess a common metasomatic component that was re-mobilised by later melts during their migration towards the surface. This could explain the compositional similarities between the arc lavas and the metasomatised peridotites, but does not offer new insights to decipher the relationships among erupted adakites and the sub-arc peridotite mantle (Defant and Kepezhinskas, 2001).

In this respect, the lack of glass melts resembling adakites is unexpected and makes the Grenada xenoliths unique. The origin of adakites found at surface has been related to slab melting, related potentially to the unique tectonics of the southern terminus of the Lesser Antilles where Grenada resides (Defant et al., 2000). These melts are expected to react with host mantle during their migration towards the surface. Thus, mantle xenoliths should bear the unique signatures of this metasomatism as documented elsewhere (Schiano et al., 1995; Defant and Kepezhinskas, 2001; Prouteau et al., 2001). Melts low in HREE and Y relative to the LREE (adakites) have been reported in xenoliths from the Batan arc, Philippines (Schiano et al., 1995), the Kamchatka arc (Kepezhinskas et al., 1995, 1996), and the Austral Andean arc (Stern and Kilian, 1996). As discussed above, the Grenada silica-rich interstitial melt inclusions resemble adakites in their high Si, Al, and Sr but do not have low Y or HREE. We have had to conclude that these melts are due to in-situ melting, but our

sampling of interstitial glass inclusions was limited to two harzburgite samples and inclusions large enough to analyse. Further studies may uncover the presence of adakitic melts. Alternatively, we have to speculate either that at Grenada adakites migrate from their source regions along major lithospheric fractures or that their metasomatic charge cannot be easily recognised in the shallower lithospheric mantle because it was progressively lost during the migration towards the surface.

One thing is clear: Grenada is extremely unique in its variety of rocks including calc-alkaline and alkalic suites of volcanic rocks, adakites and mantle xenoliths. No where is there anything like them in the Lesser Antilles arc, and most arcs bear nothing similar. The unique compilation of lavas may require a unique tectonic and petrogenetic scenario.

Acknowledgments

Funding for this work was provided by the Ministero dell'Università e della Ricerca Scientifica e Tecnologica (PRIN 2005 project "Migrazione e messa in posto di fusi mantellici nella litosfera") to Riccardo Tribuzio and by the Consiglio Nazionale delle Ricerche to the IGG-Pavia. This manuscript was improved following the reviews by R. Arculus, C. Szabó and O. Müntener.

References

Albee, A.L., Ray, L., 1970. Correction factors for electron probe microanalysis of silicates, oxides, carbonates, phosphates, and sulfates. Anal. Chem. 42, 1408–1414.

Anders, E., Ebihara, M., 1982. Solar system abundances of the elements. Geochim. Cosmochim. Acta 46, 2363–2380.

Arculus, R.J., 1976. Geology and geochemistry of the alkali basalt–andesite association of Grenada, Lesser Antilles island arc. Geol. Soc. Amer. Bull. 87, 612–624.

Arculus, R.J., Wills, K.J., 1980. The petrology of igneous blocks and inclusions from the Lesser Antilles island arc. J. Petrol. 21, 143–168.

Baker, M.B., Hirschmann, M.M., Ghiorso, M.S., Stolper, E.M., 1995. Compositions of near-solidus peridotite melts for experiments and thermodynamic calculations. Nature 375, 308–311.

Barsdell, M., Smith, I.E.M., 1989. Petrology of recrystallised ultramafic xenoliths from Merelava volcano, Vanuatu. Contrib. Mineral. Petrol. 102, 230–241.

Batanova, V.G., Suhr, G., Sobolev, A., 1998. Origin of geochemical heterogeneity in the mantle peridotites from the Bay of Islands ophiolite, Newfoundland, Canada: ion probe study of clinopyroxenes. Geochim. Cosmochim. Acta 62, 853–866.

Bedini, R.M., Bodinier, J.L., Dautria, J.M., Morten, L., 1997. Evolution of LILE-enriched small melt fractions in the lithospheric mantle: a case study from the East African Rift. Earth Planet. Sci. Lett. 153, 67–83.

Bence, A.E., Albee, A.L., 1968. Empirical correction factors for the electron microanalysis of silicates and oxides. J. Geol. 76, 382–403.

Bizimis, M., Salters, V.J.M., Bonatti, E., 2000. Trace and REE content of clinopyroxenes from supra-subduction zone peridotites. Implications for melting and enrichment processes in island arcs. Chem. Geol. 165, 67–85.

Bodinier, J.L., Vasseur, G., Vernieres, J., Dupuy, C., Fabries, J., 1990. Mechanisms of mantle metasomatism: geochemical evidence from the Lherz orogenic peridotite. J. Petrol. 31, 597–628.

Brenan, J.M., Shaw, H.F., Ryerson, F.J., Phinney, D.L., 1995. Mineral–aqueous fluid partitioning of trace elements at 900 °C and 2.0 GPa: constraints on the trace element chemistry of mantle and deep crustal fluids. Geochim. Cosmochim. Acta 59, 3331–3350.

Brey, G.P., Köhler, T., 1990. Geothermobarometry in four-phase lherzolites; II. New thermobarometers, and practical assessment of existing thermobarometers. J. Petrol. 31, 1353–1378.

Briden, J.C., Rex, D.C., Faller, A.M., Tomblin, J.F., 1979. K–Ar geochronology and paleomagnetism of volcanic rocks in the Lesser Antilles island arc. Philos. Trans. R. Soc. Lond. 291, 485–528.

Conrad, W.K., Kay, R.W., 1984. Ultramafic and mafic inclusions from Adak Island: crystallization history, and implications for the nature of primary magmas and crustal evolution in the Aleutian Arc. J. Petrol. 25, 88–125.

Debari, S.M., Mahlburg Kay, S., Kay, R.W., 1987. Ultramafic xenoliths from Adagdak volcano, Adak, Aleutian Island, Alaska: deformed igneous cumulates from the moho. J. Geol. 95, 329–341.

Defant, M.J., Kepezhinskas, P.K., 2001. Evidence suggests slab melting in arc magmas. EOS 82, 65–69.

Defant, M.J., Kepezhinskas, P.K., de Boer, J., 2000. Slab melting at the Southern Terminus of the Lesser Antilles Arc: the petrology, geochemistry and tectonics of the Grenada Region. AGU Fall Meeting, EOS vol. 81, F1289.

DeLong, S.E., Hodges, F.N., Arculus, R.J., 1975. Ultramafic and mafic inclusions, Kanaga Island, Alaska, and the occurrence of alkaline rocks in island arcs. J. Geol. 83, 721–736.

Dick, H.J.B., 1989. Abyssal peridotites, very slow spreading ridges and ocean ridge magmatism. Spec. Publ. - Geol. Soc. 42, 71–105.

Eiler, J.M., McInnes, B., Valley, J.W., Graham, C.M., Stolper, E.M., 1998. Oxygen isotope evidence for slab-derived fluids in the sub-arc mantle. Nature 393, 777–781.

Grégoire, M., McInnes, B.I.A., O'Reilly, S.Y., 2001. Hydrous metasomatism of oceanic sub-arc mantle, Lihir, Papua New Guinea Part 2. Trace element characteristics of slab-derived fluids. Lithos 59, 91–108.

Hart, S.R., Dunn, T., 1993. Experimental cpx/melt partitioning of 24 trace elements. Contrib. Mineral. Petrol. 113, 1–8.

Hellebrand, E., Snow, J.E., Dick, H.J.B., Hofmann, A.W., 2001. Coupled major and trace elements as indicators of the extent of melting in mid-ocean-ridge peridotites. Nature 410, 677–681.

Hirschmann, M.M., Baker, M.B., Stolper, E.M., 1998. The effect of alkalis on the silica content of mantle-derived melts. Geochim. Cosmochim. Acta 62, 883–902.

Ishii, T., Robinson, P.T., Maekawa, H., Fiske, R., 1992. Petrological studies of peridotites from diapiric serpentinite seamounts in the Izu–Ogasawara–Mariana forearc, Leg 125. Proc. Ocean Drill. Program Sci. Results 125, 445–485.

Johnson, K.T.M., 1990. Melting in the oceanic upper mantle: an ion microprobe study of diopsides in abyssal peridotites. J. Geophys. Res. 94, 2661–2678.

Kepezhinskas, P.K., Defant, M.J., 1996. Contrasting styles of mantle metasomatism above subduction zones: constraints from ultramafic xenoliths in Kamchatka. In: Bebout, G., et al. (Ed.), Subduction Top to Bottom: AGU Geophysical Monograph Monograph Series vol. 96, 307–314.

Kepezhinskas, P., Defant, M.J., 2001. Nonchondritic Pt/Pd ratios in arc mantle xenoliths: evidence for platinum enrichment in depleted island-arc mantle sources. Geology 29, 851–854.

Kepezhinskas, P.K., Defant, M.J., Drummond, M.S., 1995. Na metasomatism in the island-arc mantle by slab melt–peridotite interaction: Evidence from mantle xenoliths in the north Kamchatka arc, Russia. J. Petrol. 36, 1505–1527.

Kepezhinskas, P., Defant, M.J., Drummond, M.S., 1996. Progressive enrichment of island arc mantle by melt–peridotite interaction inferred from Kamchatka xenoliths. Geochim. Cosmochim. Acta 60, 1217–1229.

Kepezhinskas, P., Defant, M.J., Vannucci, R., Tiepolo, M., 2000. Ultramafic xenoliths from Grenada, Lesser Antilles: evidence for slab melt–mantle wedge interaction and adakitic (Na) metasomatism. AGU Fall Meeting, EOS, vol. 81, F1290.

Kepezhinskas, P., Defant, M.J., Widom, E., 2002. Abundance and distribution of PGE and Au in the island-arc mantle: implications for sub-arc metsomatism. Lithos 60, 113–128.

Keppler, H., 1996. Constraints from partitioning experiments on the composition of subduction-zone-fluids. Nature 380, 237–240.

Kessel, R., Schmidt, M.W., Ulmer, P., Pettke, U., 2005. Trace element signature of subduction-zone fluids, melts and supercritical liquids at 120–180 km depth. Nature 437, 724–727.

Maury, R.C., Defant, M.J., Joron, J.L., 1992. Metasomatism of the sub-arc mantle inferred from trace elements in Philippine xenoliths. Nature 360, 661–663.

McCulloch, M.T., Gamble, J.A., 1991. Geochemical and geodynamical constraints on subduction zone magmatism. Earth Planet. Sci. Lett. 102, 358–374.

McInnes, B.I.A., Cameron, E.M., 1994. Carbonated, alkaline hybridizing melts from the sub-arc environment: mantle wedge samples from the Tabar–Lihir–Tanga–Feni arc, Papua New Guinea. Earth Planet. Sci. Lett. 122, 125–141.

McInnes, B.I.A., McBride, J.S., Evans, N.J., Lambert, D.D., Andrew, A.S., 1999. Osmium isotope constraints on ore metal recycling in subduction zones. Science 286, 12.

McInnes, B.I.A., Gregoire, M., Binns, R.A., Herzig, P.M., Hannington, M.D., 2001. Hydrous metasomatism of oceanic sub-arc mantle, Lihir, Papua New Guinea; petrology and geochemistry of fluid-metasomatised mantle wedge xenoliths. Earth Planet. Sci. Lett. 188, 169–183.

Navon, O., Stolper, E., 1987. Geochemical consequences of melt percolation: the upper mantle as a chromatographic column. J. Geol. 95, 285–307.

Parkinson, I.J., Arculus, R.J., 1999. The redox state of subduction zones: insights from arc-peridotites. Chem. Geol. 160, 409–423.

Parkinson, I.J., Pearce, J.A., 1998. Peridotites from the Izu–Bonin–Mariana forearc (ODP Leg 125); evidence for mantle melting and melt–mantle interaction in a supra-subduction zone setting. J. Petrol. 39, 1577–1618.

Parkinson, I.J., Arculus, R.J., Eggins, S.M., 2003. Peridotite xenoliths from Grenada, Lesser Antilles Island Arc. Contrib. Mineral. Petrol. 146, 241–262.

Parkinson, I.J., Pearce, J.A., Thirlwall, M.F., Johnson, K.T.M., Ingram, G., 1992. Trace element geochemistry of peridotites from the Izu–Bonin–Mariana forearc, Leg 125. Proc. Ocean Drill. Program Sci. Results 125, 487–506.

Pindell, J.R., Barret, S.F., 1990. Geological evolution of the Caribbean region; a plate tectonic perspective. In: Dengo, G., Case, J.E. (Eds.), The Caribbean region. . The geology of North America. Geol. Soc. Am., Boulder, CO, United States, pp. 405–432.

Prouteau, G., Scaillet, B., Pichavant, M., Maury, R., 2001. Evidence for mantle metasomatism by hydrous silicic melts derived from subducted oceanic crust. Nature 410, 197–200.

Rapp, R.P., Shimizu, N., Norman, M.D., Applegate, G.S., 1999. Reaction between slab-derived melts and peridotite in the mantle wedge: experimental constraints at 3.8 Gpa. Chem. Geol. 160, 335–356.

Rivalenti, G., Mazzucchelli, M., Laurora, A., Ciuffi, S.I.A., Zanetti, A., Vannucci, R., Cingolani, C.A., 2004. The composition and processes of the backarc mantle lithosphere in Patagonia. J. South Am. Earth Sci. 17, 121–152.

Schiano, P., Clocchiatti, R., Shimizu, N., Maury, R.C., Jochum, K.P., Hofmann, A.W., 1995. Hydrous, silica-rich melts in the sub-arc mantle and their relationship with erupted arc lavas. Nature 377, 595–600.

Speed, R.C., Russo, R.M., Foland, K.A., 1993. Cenozoic oblique collision of South American and Caribbean plates; new evidence in the Coastal Cordillera of Venezuela and Trinidad. AAPG Bull. 77, 349.

Stern, C.R., Kilian, R., 1996. Role of the subducted slab, mantle wedge and continental crust in the generation of adakites from the Andean Austral Volcanic Zone. Contrib. Mineral. Petrol. 123, 263–281.

Swanson, S.E., Kay, S.M., Brearley, M., Scarfe, C.M., 1987. Arc and back arc xenoliths in Kurile–Kamchatka and western Alaska. In: Nixon (Ed.), In Mantle Xenoliths. John Wiley and Sons, New York, pp. 303–318.

Thirlwall, M.F., Graham, A.M., 1984. Evolution of high-Ca, high-Sr C-series basalt from Grenada, lesser Antilles: the effects of the intra-crustal contamination. J. Geol. Soc. (Lond.) 141, 427–445.

Thirlwall, M.F., Graham, A.M., Arculus, R.J., Harmon, R.S., Macpherson, C.G., 1996. Resolution of the effects of crustal assimilation, sediment subduction and fluid transport in island arc magmas: Pb–Sr–Nd–O isotope geochemistry of Grenada, Lesser Antilles. Geochim. Cosmochim. Acta 63, 4785–4810.

Tiepolo, M., Bottazzi, P., Palenzona, M., Vannucci, R., 2003. A laser probe coupled with ICP-double focusing sector-field mass spectrometer for in-situ analysis of geological samples and U–Pb dating of zircon. Can. Mineral. 41, 259–272.

Vernières, J., Godard, M., Bodinier, J.L., 1997. A plate model for the simulation of trace element fractionation during partial melting and magma transport in the Earth's upper mantle. J. Geophys. Res. 102, 24,771–24,784.

Vidal, P.H., Dupuy, C., Maury, R., Richard, M., 1989. Mantle metasomatism above subduction zones: trace-element and radiogenic isotope characteristics of peridotite xenoliths from, Batan Island Philippines. Geology 17, 1115–1118.

Waggoner, G., 1987. Proposed drilling sites in the Caribbean Sea. Caribbean Geological Evolution; Report of a Workshop to Define Caribbean Geological Problems, Needed Investigations, and Initiatives for Ocean Drilling, pp. 167–169.

Wells, P.R.A., 1977. Pyroxene thermometry in simple and complex systems. Contrib. Mineral. Petrol. 62, 129–139.

Wood, B.J., Banno, S., 1973. Garnet–orthopyroxene and orthopyroxene–clinopyroxene Relationships in simple and complex systems. Contrib. Mineral. Petrol. 42, 109–124.

Woodland, S.J., Pearson, D.G., Thirlwall, M.F., 2002. A platinum group element and Re–Os isotope investigation of siderophile element recycling in subduction zones: comparison of Grenada, Lesser Antilles arc, and the Izu–Bonin arc. J. Petrol. 43, 171–198.

Wulff-Pedersen, E., Neumann, E.R., Vannucci, R., Bottazzi, P., Ottolini, L., 1999. Silicic melts produced by reaction between peridotite and infiltrating basaltic melts: ion probe data on glasses

and minerals in veined xenoliths from La Palma, Canary islands. Contrib. Mineral. Petrol. 137, 59–82.

Xu, Y.G., Menzies, M.A., Bodinier, J.L., Bedini, R.M., Vroon, P., Mercier, J.C., 1998. Melt percolation and reaction atop a plume: evidence from the poikiloblastic peridotite xenoliths from Borée (Massif Central, France). Contrib. Mineral. Petrol. 132, 65–84.

Zinngrebe, E., Foley, S.F., 1995. Metasomatism in mantle xenoliths from Gees, West Eifel, Germany: evidence for the genesis of calc-alkaline glasses and metasomatic Ca-enrichment. Contrib. Mineral. Petrol. 122, 79–96.